IOPscience iopscience.iop.org

Home Search Collections Journals About Contact us My IOPscience

A Novel Dual-Rotor Turbine for Increased Wind Energy Capture

This content has been downloaded from IOPscience. Please scroll down to see the full text.

2014 J. Phys.: Conf. Ser. 524 012078

(http://iopscience.iop.org/1742-6596/524/1/012078)

View the table of contents for this issue, or go to the journal homepage for more

Download details:

IP Address: 129.186.252.111
This content was downloaded on 10/07/2014 at 16:13

Please note that terms and conditions apply.

A Novel Dual-Rotor Turbine for Increased Wind Energy Capture

A Rosenberg, S Selvaraj, and A Sharma

Department of Aerospace Engineering, Iowa State University, Ames, Iowa, 50011, USA.

E-mail: sharma@iastate.edu

Abstract. Horizontal axis wind turbines suffer from aerodynamic inefficiencies in the blade root region (near the hub) due to several non-aerodynamic constraints. Aerodynamic interactions between turbines in a wind farm also lead to significant loss of wind farm efficiency. A new dual-rotor wind turbine (DRWT) concept is proposed that aims at mitigating these two losses. A DRWT is designed that uses an existing turbine rotor for the main rotor, while the secondary rotor is designed using a high lift-to-drag ratio airfoil. Reynolds Averaged Navier-Stokes computational fluid dynamics simulations are used to optimize the design. Large eddy simulations confirm the increase energy capture potential of the DRWT. Wake comparisons however do not show enhanced entrainment of axial momentum.

1. Introduction

A single-rotor horizontal axis wind turbine (HAWT) can capture a maximum of 59.3% of the flow energy passing through the turbine rotor disk. This remarkable result can be derived by applying mass, momentum, and energy conservations laws across a rotor disk assuming the flow to be one-dimensional, steady, and incompressible. This limit was found at around the same time by Albert Betz, Frederick Lanchester, and Nikolay Zhukovsky, but is now referred to simply as the Betz limit. It should be emphasized that this limit assumes the turbine to have a single, un-ducted rotor. On one hand, this limit can be easily surpassed if multiple rotors, or ducted rotors are employed. On the other hand, the Betz limit of achieving 59.3% aerodynamic efficiency is not realizable by any real single-rotor, finite-bladed, un-ducted HAWT. Physical laws and other constraints limit the efficiency to be no greater than around 53% (see Fig. 1). Figure 1 postulates an alternate, more practical limit on the maximum aerodynamic efficiency potential of modern HAWTs. Based on a representative (some form of weighted average) lift-to-drag ratio (C_l/C_d) for entire turbine rotor, this practical limit is drawn as a $C_P - \lambda$ curve (shown in blue for $C_l/C_d = 100$) in Fig. 1. C_P is the non-dimensional power (Betz limit is $C_P = 0.593$) and λ is the ratio of blade tip speed to freestream wind speed.

Maximum C_P of modern utility-scale HAWT's is only a few percentage points short of this practical limit. A good portion of this shortfall is due to aerodynamic losses in blade root region. Rotor blades in the root region (approximately bottom 25% of a rotor) is designed to withstand blade root bending moments. For structural integrity, relatively thick (high thickness-to-chord ratio) airfoils are chosen in the root region, which are aerodynamically poor. Flow separation in the root region causes span-wise (cross) flow, which deteriorates the aerodynamic performance of the outboard blade sections as well. Blade thickness, twist, and chord in the root region are


Content from this work may be used under the terms of the Creative Commons Attribution 3.0 licence. Any further distribution of this work must maintain attribution to the author(s) and the title of the work, journal citation and DOI.
Published under licence by IOP Publishing Ltd

limited by structural, manufacturing, and transportation limitations. A systematic diagnostic study by Sharma [2] has revealed that these constraints reduce turbine aerodynamic efficiency by about 5%. In this paper, we present a novel turbine concept to mitigate these root losses.

Utility scale turbines are deployed in clusters called wind farms. It is now recognized by the wind energy community that these turbines cannot be studied and/or optimized as if operating in isolation. Aerodynamic interaction between turbines in wind farms results in significant energy loss that ranges anywhere between 8-40% [3]. The primary mechanism of this energy loss is ingestion (by downstream turbines) of reduced-momentum air present in the wakes of upstream turbines. The range of this loss is exceptionally wide because of its strong dependence on farm location, layout (micro-siting), and atmospheric stability. Highest losses have been observed in offshore turbines when turbine rows are aligned with wind direction, are closely spaced, and when atmospheric flow is stably stratified [4, 5]). In comparison to the large body of work devoted to measuring and predicting wake losses, relatively little research has focused on reducing wake losses. For HAWTs, Corten and Lindenburg [6] have developed a method of farm control in which windward turbines are deliberately yawed (skewed) with respect to wind direction. The concept is to use the lateral force (generated by deliberate yawing of windward turbines) to divert the flow away from downstream turbines. The degree of yaw is determined based on wind and turbine row alignment.

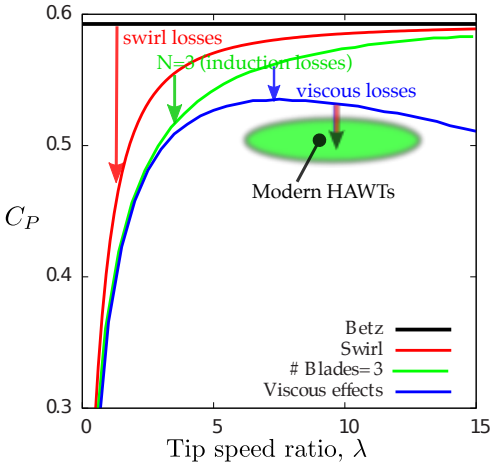

Figure 1: Maximum possible C_P with various approximations (Selvaraj *et al* [1]).

With the wind energy industry fixated on single-rotor HAWT designs, primarily from cost considerations, multi-stage designs (e.g., dual-rotor turbines, DRWTs) have received little attention. Multi-stage turbomachines are widely used in the gas turbine industry, where fuel has a price and hence, efficiency is prime. "Fuel" in wind turbines is supposedly free. Therefore, cost of electricity production, rather than efficiency, drives current turbine designs. As we approach the inevitability of having to produce most of our energy sustainably, with wind playing a substantial role in this quest, we will run out of sites (land or sea) where we can realistically install turbines [7]. The focus has to therefore shift towards efficient turbine and farm designs that extract highest power per square meter of surface area.

Multi-rotor turbines can surpass the Betz limit (applicable only for single rotor wind turbines, SRWTs). The Rankine-Froude momentum theory, used to compute the Betz limit, was extended to study multi-rotor turbines by Newman [8]. Newman [8] calculated the maximum C_P of an equal-size DRWT to be 0.64, an 8% improvement over the Betz limit. Further addition of rotor stages gives diminishing returns. It is because of the added cost (rotor blades are the costliest part of a turbine) and the complexity (additional drivetrain, gearbox, etc.) that multi-rotor turbines are not widely used.

Jung *et al* [9] numerically investigated the performance of a 30 kW counter-rotating DRWT and calculated optimum values for axial separation between primary and secondary rotors, and secondary rotor size. Lee *et al* [10, 11] investigated effects of design parameters such as combination of pitch angles, rotating speed ratio, and radius ratio (between primary and secondary rotors) on a DRWT. They found that maximum C_P occurs when front rotor size was chosen to be 80% of the second rotor. Kumar et al. [12] compared aerodynamic performances of DRWT against conventional, single-rotor HAWTs using CFD. A few DRWT prototypes have also been built and tested. Windpower Engineering & Development has developed a co-axial,

twin-rotor turbine with the objective of harvesting more energy at lower wind speeds. They use two identical rotors connected by one shaft to a variable-speed generator. Enercon also has a patent [13] on a dual-rotor concept similar to the one proposed here, however it is focused on growing rotor radius rather than reducing losses.

A dual-rotor turbine concept (see Fig. 2) is proposed and investigated here. In this dual-rotor concept, a smaller, aerodynamically tailored, secondary co-axial rotor is placed ahead of the main rotor. None of the DRWT articles referenced above focus on what we are targeting with the proposed DRWT concept. Our goals are: (1) reduce root losses, and (2) reduce wake losses in a wind farm through enhanced wake mixing. The first goal targets improving isolated turbine efficiency through the use of aerodynamically optimized secondary rotor. The second goal targets efficiency improvement at wind-farm scale by (a) tailoring rotor wake shear, and (b) by exploiting dynamic interaction between vortices from main and secondary rotors of a DRWT.

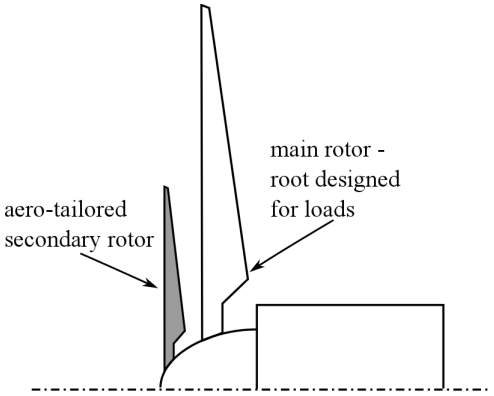

Figure 2: A schematic of the proposed dual-rotor concept.

2. Numerical Methods

Wind turbine and wind farm aerodynamics can be modeled with a spectrum of tools that vary considerably in fidelity and computational complexity (cost). Analytical [14, 15] and semi-analytical models [16], parabolic wake models [17], Reynolds Averaged Navier-Stokes (RANS) simulations [18], and Large Eddy Simulations (LES), all play different, yet necessary roles in turbine/farm analysis and design. Vermeer [19] and Sanderse [20] provide excellent reviews of various numerical methods available to study wind turbine and wind farm aerodynamics.

Two numerical models are used to analyze aerodynamics of DRWTs. Reynolds Averaged Navier Stokes (RANS) simulations with a generalized actuator disk parameterization of turbine rotors are performed to carry out preliminary design iterations towards optimizing aerodynamic performance. The optimized DRWT turbine is analyzed with a Large Eddy Simulations (LES) model to investigate turbine wake evolution and compare it with that of a SRWT.

2.1. Rotor Parameterization using Actuator Disk/Line/Surface Models

Numerical modeling of wind turbine/farm aerodynamics can be classified into two categories based on whether or not rotor geometry is resolved. When the relevant length scale in the problem is smaller or comparable to blade chord (e.g., in dynamic load computations, or very near wake calculations), resolving blade geometry is essential. Vijaykumar *et al* [21] and Lavely *et al* [22] present recent results from the Cyber wind facility at Penn State. They insist that resolving the flow near the blades is necessary for evaluating fatigue loads. They promote the use of blade-resolved URANS-LES calculations. However, in investigations of turbine wake evolution or wind farm aerodynamics, resolving rotor blades is arguably unnecessary. The effect of rotors on wake flows in such simulations is represented through sources in the momentum equation. This source representation can be in the form of disk (actuator disk), line (actuator line), or surface (actuator surface). Sørensen [23] and Mikkelsen [24] nicely summarize these methods. Porté-Agel *et al* [25] and Wu and Porté-Agel [26] evaluated relative accuracy of three different actuator representations of turbine rotors in CFD and demonstrated the importance of including in-plane rotor forces with these models.

2.2. Reynolds Averaged Navier Stokes (RANS) Simulations

A generalized actuator disk model is implemented in OpenFOAM to analyze HAWT aerodynamics. OpenFOAM is essentially a group of C++ libraries used to create solvers. The SimpleFOAM solver (a part of OpenFOAM software suite) is used in the present study. SimpleFOAM solves the incompressible RANS equations,

$$\frac{\partial \bar{u}_i}{\partial x_i} = 0, \text{ and,} \tag{1}$$

$$\bar{u}_j \frac{\partial \bar{u}_i}{\partial x_j} = -\frac{1}{\rho}\frac{\partial \bar{p}}{\partial x_i} + \nu \frac{\partial^2 \bar{u}_i}{\partial {x_j}^2} - \frac{\partial \overline{u_i' u_j'}}{\partial x_j} + \frac{f_i}{\rho}, \tag{2}$$

where the Reynolds stress tensor, $\overline{u_i' u_j'}$ is modeled using eddy ("turbulent") viscosity as $\nu_t \partial \overline{u_i}/\partial x_j$. Turbulent viscosity, ν_t is obtained using turbulent kinetic energy, k and dissipation, ϵ, which are themselves obtained by solving a transport equation for each. The term f_i represents body force per unit volume and is obtained using airfoil polars and local flow velocity. The force, f_i is distributed over a volume and a Gaussian distribution is applied along the flow direction following Mikkelsen [24]. This model has been previously validated against experimental data as well as the Blade Element Momentum (BEM) theory solutions for single-rotor turbines [1]; sample validation results are shown in Fig. 3.

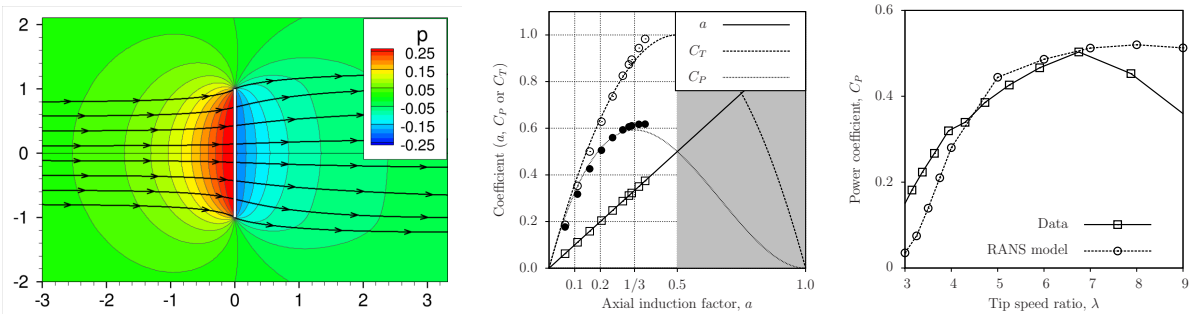

(a) Pressure contours (b) 1-D momentum theory (c) Risø turbine

Figure 3: Wind turbine aerodynamics simulation results. Validation shown in (b) and (c).

2.3. Large Eddy Simulations

Modeling wind turbine and wind farm aerodynamics using LES has received a lot of research attention in recent years (see e.g., [25, 26, 27, 28, 29]). The Simulator for Offshore Wind Farm Application (SOWFA) [30, 31] software is used here. In this LES model, spatially filtered, incompressible forms of continuity and Navier-Stokes equations are solved using spatial and temporal discretization. Spatial filtering introduces unresolved, sub-filter scale (also called sub-grid scale or SGS) stresses, which have to be modeled. The width of the spatial filter is taken to be the grid-filter width given by $\Delta = (\Delta_x \Delta_y \Delta_z)^{1/3}$. The actuator line model (ALM) is used for rotor parameterization. Denoting spatially-filtered quantities by ($\tilde{}$), the governing fluid flow

equations are

$$\begin{aligned}
\frac{\partial \widetilde{u_i}}{\partial x_i} &= 0, \\
\frac{\partial \widetilde{u_i}}{\partial t} + \widetilde{u_j}\left(\frac{\partial \widetilde{u_i}}{\partial x_j} - \frac{\partial \widetilde{u_j}}{\partial x_i}\right) &= -\frac{\partial \widetilde{p^*}}{\partial x_i} - \frac{\partial \tau_{ij}}{\partial x_j} + \nu\frac{\partial^2 \widetilde{u_i}}{\partial x_j^2} \\
&- \underbrace{f_i/\rho_0}_{\text{turbine force}} + \underbrace{\delta_{i1}F_P}_{\text{driving pressure}} + \underbrace{\delta_{i3}g_0(\widetilde{\theta} - \langle\widetilde{\theta}\rangle)/\theta_0}_{\text{buoyancy force}} + \underbrace{F_c\epsilon_{ij3}\widetilde{u_j}}_{\text{coriolis force}}, \\
\frac{\partial \widetilde{\theta}}{\partial t} + \widetilde{u_j}\frac{\partial \widetilde{\theta}}{\partial x_j} &= -\frac{\partial q_j}{\partial x_j} + \alpha\frac{\partial^2 \widetilde{\theta}}{\partial x_j^2},
\end{aligned}$$

where, $\widetilde{p^*} = \widetilde{p}/\rho_0 + \widetilde{u_i}\widetilde{u_j}/2$ is the modified kinematic pressure, $\tau_{ij} = \widetilde{u_i u_j} - \widetilde{u_i}\widetilde{u_j}$, is sub-grid scale (SGS) stress tensor, and $q_j = \widetilde{u_j\theta} - \widetilde{u_j}\widetilde{\theta}$ is SGS heat flux. f_i is momentum source to model forces exerted by turbine blades, $\delta_{i1}F_P$ is pressure gradient to drive flow, θ is potential temperature and α is thermal diffusivity of the fluid. The deviatoric part of the SGS stress tensor, τ_{ij} is typically modeled using an eddy-viscosity model, $\tau_{ij} - 1/3\ \delta_{ij}\tau_{kk} = -2\nu_{sgs}\widetilde{S_{ij}}$ and the SGS heat flux with an eddy-diffusivity model $q_j = \widetilde{u_j\theta} - \widetilde{u_j}\widetilde{\theta} = -(\nu_{sgs}/Pr_{sgs})\partial\widetilde{\theta}/\partial x_j$, where, $\widetilde{S_{ij}} = 1/2\ (\partial\widetilde{u_i}/\partial x_j + \partial\widetilde{u_j}/\partial x_i)$ is the resolved strain-rate tensor and Pr_{sgs} is the SGS Prandtl number. The mixing-length model by Smagorinsky [32], $\nu_{sgs} = (C_S\Delta)^2|\widetilde{S}|$ is used to model ν_{sgs}.

3. Dual-Rotor Simulations

The RANS method described in the previous section can be directly used to simulate dual-rotor wind turbine aerodynamics. The two rotors of a DRWT are modeled as two different, independent single-rotor turbines. It should be borne in mind that the two rotors of a DRWT are in close proximity, with a consequence that the potential field (due to finite blade thickness) of one rotor can affect the other. Stagnation pressure created near the leading and trailing edges of the main rotor, for example, can influence the aerodynamics of the secondary rotor. Such potential field interaction is not modeled here due to parameterization of rotors by actuator disk/line methods. While the potential field interaction cannot be completely ignored, we believe that a conceptual evaluation of the DRWT concept, such as proposed here, can be conducted with this simplification. Also, hub/nacelle geometry as well as turbine tower are not modeled in these simulations. The effect of hub/nacelle on flow in the root region is not negligible, but is ignored in the present simulations to avoid confounding effects. The simulations assume axisymmetric flow and the CFD domain is therefore only 1 cell thick in the circumferential direction. The domain extends 10 rotor radii upstream and downstream as well as in the radial direction. The average number of cells for these simulations is 22 K.

The ability of the RANS model to simulate multiple rotors is first verified for a canonical case by comparing against analytical results for a four, equal-size and uniformly loaded rotors (disks) by Newman [8]. The simulation is run by specifying the thrust coefficient for each rotor disk for maximum C_P for the entire turbine. Figure 4 compares CFD predicted C_P with analytical results. Fair agreement is observed between theory and simulations although the simulations in general predict higher power for downstream disks (#3 & #4) and lower power for upstream disks (#1 & #2). This is perhaps

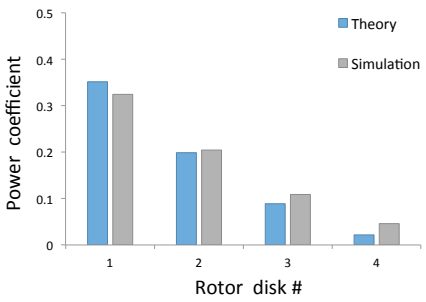

Figure 4: Comparison of numerically predicted and analytically evaluated (by Newman [8]) C_P.

because of the turbulent mixing present in the simulations which reduces the wake deficit into the downstream turbines. The analytical results ignore wake mixing. Comparisons were also made for two-disk and three-disk turbines with similar accuracy.

3.1. Rotor Design

Preliminary design of the secondary rotor of a DRWT is carried out using an inverse design approach based on the blade element momentum theory. This approach is similar to one of the approaches used in PROPID [33, 34]. For design purpose, the secondary rotor is assumed to be operating in isolation (i.e., the effect of the primary rotor is ignored). The secondary rotor blades are designed with the DU96 airfoil, which is a high lift-to-drag ratio airfoil typically used for designing tip sections of main rotor blades. An aerodynamically optimum (for an isolated rotor) design is sought. Therefore, uniform axial induction, $a = 1/3$ and uniform lift coefficient, $C_l = 0.81$ (corresponding to the C_l value where maximum lift-to-drag ratio, C_l/C_d occurs) are prescribed. The inverse design approach then yields radial distributions of blade chord and twist (see Fig. 5. The lengths are normalized by the secondary rotor tip radius in the figure.

The main rotor is chosen to be that of the conceptual 5 MW offshore NREL turbine [35]. These blade designs remain non-dimensionally unchanged and the optimization study, described in the next section, focuses on identifying the aerodynamically optimum physical size of the secondary rotor and the separation distance between the two rotors.

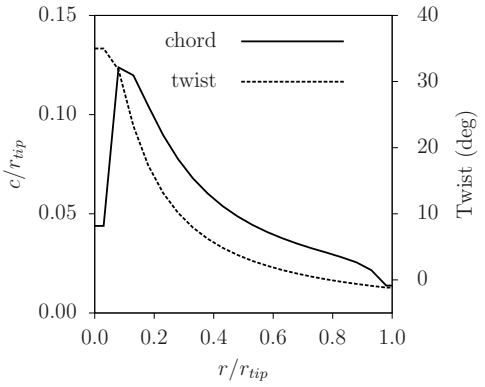

Figure 5: Radial distributions of secondary rotor blade chord and twist.

3.2. Optimization Study

The RANS modeling approach with an actuator disk representation of a turbine rotor (see Sec. 2) is used to carry out parametric sweeps as part of an optimization study. The objective is to identify a design that gives highest C_P at one operating point (defined by specifying the tip speed ratios of the two rotors). The results presented here focus on a counter-rotating design (i.e., the two rotors rotate in opposite directions). Simulations with co-rotating turbine designs gave similar but slightly less efficient designs. The tip speed ratio of the main rotor is kept fixed at 7.55 and blade pitch of 0.0, which correspond to the maximum efficiency point of the main rotor. Three parameters are varied; these are: (1) the secondary rotor diameter, (2) the axial spacing between the main and secondary rotors, and (3) the tip speed ratio of the secondary rotor. Two 2-D parametric sweeps are carried out.

In the first parametric sweep, the secondary rotor size and tip speed ratio are varied while holding fixed the axial spacing between the main and secondary rotors (at 0.5 × main rotor tip radius). Figure 6 shows some results from this study. Since the design of the main rotor is held fixed, C_P does not monotonically increase with increasing secondary rotor size. In fact, the DRWT design shows a penalty for several combinations of secondary rotor size and tip speed ratio. High penalty at large secondary rotor size and tip speed ratios is because of the secondary rotor operating too far off from its design tip speed ratio. An island of relatively large increase in C_P is found centered approximated around secondary rotor tip radius of 0.25 (× main rotor tip radius) and tip speed ratio of 6.

In the second parametric sweep, the axial spacing and the secondary rotor tip speed ratio are varied while holding the secondary rotor tip radius at the optimum value of 0.25 (× main rotor tip radius) found in the first parametric sweep. Results from this parametric study are shown in Fig. 7. A net benefit is observed for a wide range of parametric values. Figure 7 (b)

suggests that a separation distance of around 0.2 × main rotor radius would give the largest improvement in C_P over a single-rotor HAWT.

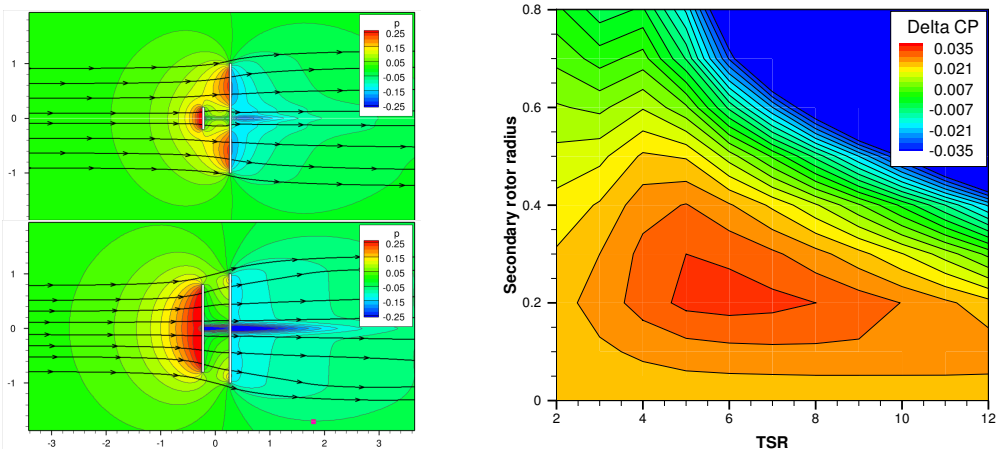

(a) Simulations for two rotor sizes (b) ΔC_P (DRWT - SRWT)

Figure 6: RANS simulation results: (a) pressure contours and streamlines for two secondary rotor sizes, and (b) difference in aerodynamic power coefficient, $\Delta C_P = C_{P\mathrm{DRWT}} - C_{P\mathrm{SRWT}}$ due to the addition of a secondary rotor.

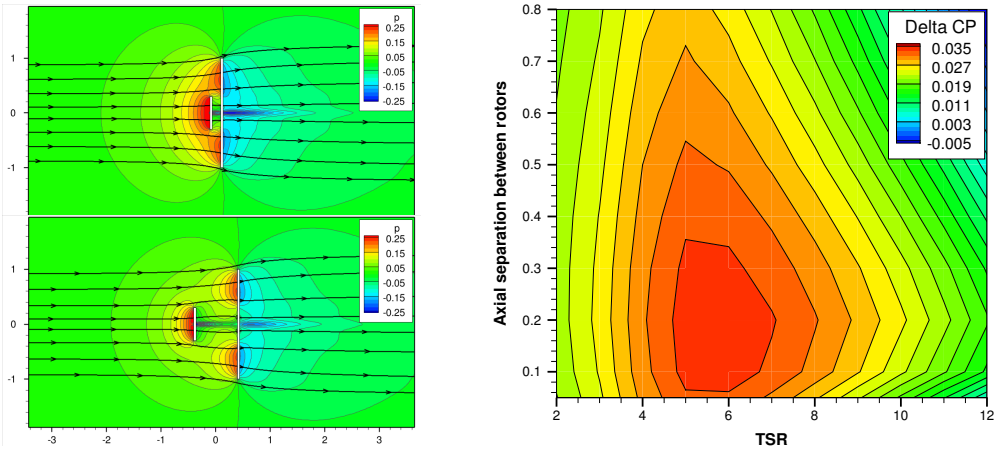

(a) Two separation distances (b) ΔC_P (DRWT - SRWT)

Figure 7: RANS simulation results: (a) pressure contours and streamlines for two axial separation distances, and (b) difference in aerodynamic power coefficient, $\Delta C_P = C_{P\mathrm{DRWT}} - C_{P\mathrm{SRWT}}$ due to the addition of a secondary rotor.

The RANS based optimization study suggest that an increase in C_P of about 0.035, which is about a 7% increase in aerodynamic efficiency, is attainable with the DRWT concept. This improvement is primarily due to efficient extraction of energy flowing near the hub of the main rotor, but in part also due to the addition of another energy extracting device. Note also that this improvement is solely on isolated rotor basis. We anticipate that the DRWT concept can also be used to mitigate wake losses, which can improve wind farm efficiency. To investigate DRWT wake behaviour, we use the LES methodology described in Sec. 2. For the LES simulations a nearly optimal secondary rotor design: tip radius = 0.3 × main rotor tip radius, axial separation = 0.2 × main rotor tip radius, and tip speed ratio, $\lambda = 6$ is selected.

3.3. Large Eddy Simulations

Large eddy simulations are carried out for the optimum DRWT configuration identified through the optimization study described in the previous section. A SRWT simulation with only the main rotor of the optimized DRWT configuration is also performed to enable a comparative study. Simulations are carried out in a computational domain that is 6D long, 4D wide and 4D tall, where D is the main rotor diameter. Figure 8 shows the computational domain dimensions and the relative placement of the turbine. Only the rotors of the turbine are simulated; the hub/nacelle and the tower were ignored in these simulations. OpenFOAM's blockMesh utility is used to create a structured mesh with $600 \times 200 \times 200$ cells. The mesh is clustered near the turbine rotors and the grid gradually stretched in the axial direction away from the rotors.

Periodic boundary conditions are used on all side boundaries, essentially simulating an infinite planar array of turbines rather than a single turbine. This should be borne in mind because far downstream from the array, the neighboring turbines will influence the wake evolution. Inflow and outflow boundary conditions are applied at the inlet and outlet boundaries. The domain is decomposed spatially using the *scotch* algorithm and simulations are performed in parallel using SOWFA. Each simulation is run for a total of 200 seconds of physical time with a constant inflow wind speed of 8 m/s. Approximating the average axial induction factor to be 0.33, the turbine wake convects downstream a distance of about 8.5 main rotor diameters in 200 seconds, so it would completely sweep the computational domain. Each simulations takes about 750 CPU hours running in parallel on 32 Intel Xeon E5-2680 processors. The E5-2680 is a 64 bit processor with 8 cores and has a clock speed of 2.7 GHz.

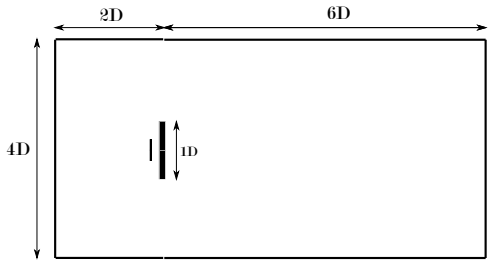

Figure 8: Domain size for the LES runs.

Figure 9 shows a snapshot in time of iso-surfaces of Q-criterion. The tip vortices from both the primary and secondary rotors are clearly visible in Fig. 9. The DRWT produces about 4.55% additional power compared to the SRWT. The secondary rotor of the DRWT produces about 6.4% of the total power. Since the main rotor operates in partial wake of the secondary rotor, it produces slightly less (98.26%) power in the DRWT configuration than in the SRWT configuration.

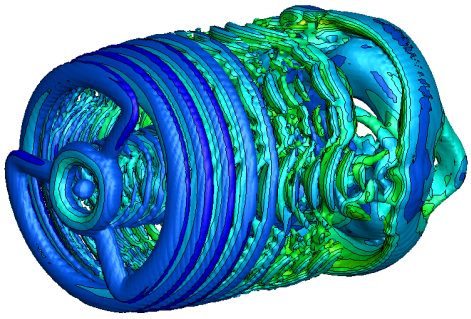
Figure 9: A snapshot of iso-surfaces of Q-criterion from the DRWT LES simulation.

To compare DRWT and SRWT wake evolution, the field variables are averaged over 50 secondary from $t = 150$ to 200 seconds. Since the turbine is abruptly started at $t = 0$, the initial data contains transients which are allowed to pass through the domain before starting data averaging. Since the incoming flow is uniform, the results can be azimuthally averaged and analyzed as functions of radius and downstream distance. Figure 10 compares the time and space (around the azimuth) averaged axial component of wind speed in the wakes of the DRWT and SRWT turbines. The velocities are compared at four different distances downstream of the turbines: 1-, 2-, 3-, and 4-main rotor diameters. The larger velocity deficit near the hub ($r/r_{tip} < 0.4$) in the case of the DRWT is due to the secondary rotor of the DRWT efficiently extracting energy from the air flowing through that region. The DRWT results also show high radial mixing in the secondary rotor slipstream. However, little-to-no evidence of enhanced radial momentum transport is observed near $r = r_{tip}$ in these results. Figure 11 compares radial variation of azimuthally

averaged turbulence intensity at four downstream distances. Higher turbulence intensity near the hub for the DRWT is consistent with the observed higher velocity deficit. Further analyses and comparisons will be carried out in the near future for turbines operating in an atmospheric boundary layer, which has a strong influence on evolution of turbine wakes.

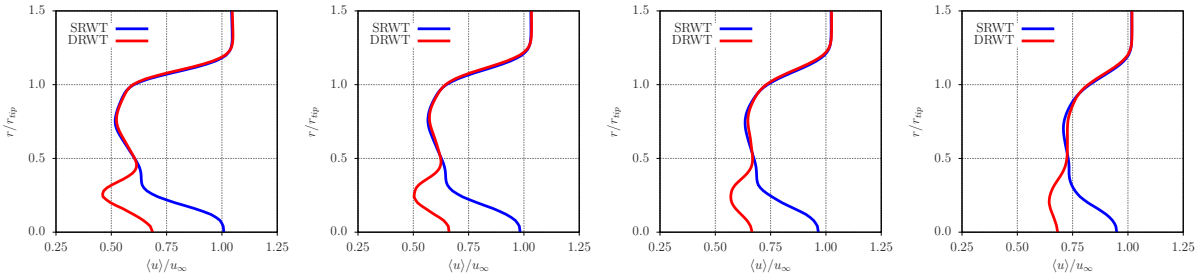

(a) $x/r_{tip} = 2$ (b) $x/r_{tip} = 4$ (c) $x/r_{tip} = 6$ (d) $x/r_{tip} = 8$

Figure 10: Radial wake variation comparisons between a single-rotor (HAWT) and a dual-rotor (DRWT) turbine at four downstream distances.

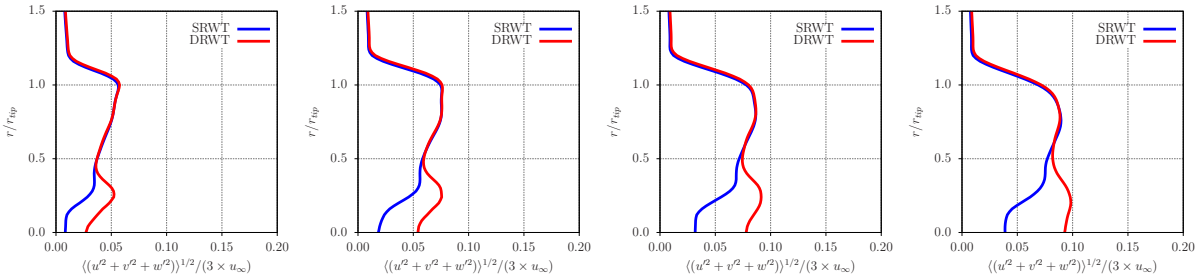

(a) $x/r_{tip} = 2$ (b) $x/r_{tip} = 4$ (c) $x/r_{tip} = 6$ (d) $x/r_{tip} = 8$

Figure 11: Radial turbulence intensity variation comparisons between a single-rotor (SRWT) and a dual-rotor (DRWT) turbine at four downstream distances.

4. Conclusions

A new dual-rotor wind turbine (DRWT) concept is presented. The secondary rotor is smaller, axially aligned with the main rotor, and designed with high lift-to-drag ratio airfoils. A DRWT is designed using the NREL 5 MW turbine as the main rotor and the secondary rotor made out of the DU96 airfoil. Parametric sweeps using RANS simulations show that secondary rotor turbine size should be 25% of the main rotor and it should be axially separated from the main rotor by a distance of 0.2 times the main rotor radius. A net benefit of 7% in C_P is predicted by RANS calculations for the optimized DRWT design. Large eddy simulations for the optimized DRWT operating in uniform flow show a net increase in power generation of about 4.6%. Wake comparisons confirm efficient extraction of energy in the root region by the DRWT. However, increase in vertical entrainment of energy, which would reduce turbine wake losses, is not clearly observed in the simulations.

5. Acknowledgment

Funding for this work was partially provided by the Iowa Energy Center under grant number 14-008-OG. The numerical simulations reported here were performed using the NSF XSEDE resources available to the authors under grant number TG-CTS130004.

References

[1] Selvaraj S, Chaves A, Takle E and Sharma A 2013 Numerical prediction of surface flow convergence phenomenon in windfarms *Proceedings of the Conference on Wind Energy Science and Technology* (METU, Ankara, Turkey: RUZGEM, Middle Eastern Technical University)
[2] Sharma A, Taghaddosi F and Gupta A 2010 Diagnosis of aerodynamic losses in the root region of a horizontal axis wind turbine (Niskayuna, New York: General Electric Internal Report)
[3] Barthelmie R J, Rathmann O, Frandsen S T, Hansen K S, Politis E, Prospathopoulos J, Rados K, Cabezn D, Schlez W, Phillips J, Neubert A, Schepers J G and van der Pijl S P 2007 *Journal of Physics: Conference Series* **75**
[4] Hansen K S, Barthelmie R J, Jensen L E and Sommer A 2012 *Wind Energy* **15** 183–196 ISSN 1099-1824
[5] Barthelmie R J and Jensen L E 2010 *Wind Energy* **13** 573–586
[6] Corten G P and Lindenburg P S 2007 Assembly of energy flow collectors, such as windpark, and method of operation uS Patent 7299627 B2
[7] Mackay D 2008 *Sustainable Energy without the hot air* (UIT Cambridge Ltd.) ISBN 0954452933
[8] Newman B 1986 *Journal of Wind Engineering and Industrial Aerodynamics* **24** 215–225
[9] Jung S N, No T S and Ryu K W 2005 *Renewable Energy* **30** 631–644
[10] Lee S, Kim H and Lee S 2010 *Current Applied Physics* **10** 339–342
[11] Lee S, Kim H Son E and Lee S 2012 *Renewable Energy* **42** 140–144
[12] Kumar P S, Abraham A, Bensingh R J and Ilangovan S 2013 *Journal of Scientific & Industrial Research* **72**
[13] Wobben A 2006 Wind power installation with two rotors in tandem uS Patent 7,074,011 B1
[14] Betz A 1919 *Schraubenpropeller mit Geringstem Energieverlust.* Ph.D. thesis Gottingen Nachrichten
[15] Goldstein S 1929 *Proceedings of the Royal Society A: Mathematical, Physical and Engineering Sciences* **123** 440–465 ISSN 1364-5021
[16] Burton T, Sharpe D, Jenkins N and Bossanyi E 2002 *Wind Energy Handbook* (John Wiley & Sons Ltd.) ISBN 0-471-48997-2
[17] Ainslie J F 1988 *Journal of Wind Engineering and Industrial Aerodynamics* **27** 213–224
[18] Snel H 2003 *Wind Energy* **6** 203–211
[19] Vermeer L J, Sørensen J N and Crespo A 2003 *Progress in Aerospace Sciences* **39**
[20] Sanderse B, Pijl S P v d and Koren B 2011 *Wind Energy*
[21] Vijayakumar G, Lavely A, Jayaraman B, Craven B and JG B 2014 Blade boundary layer response to atmospheric boundary layer turbulence on a nrel 5mw wind turbine blade with hybrid urans-les *32nd ASME Wind Energy Symposium* (National Harbor, MD)
[22] Lavely A, Vijayakumar G, Craven B, Jayaraman B, Jha P, Nandi T, Paterson E and JG B 2014 Toward a blade-resolved hybrid urans-les of the nrel 5-mw wind turbine rotor within large eddy simulation of the atmospheric boundary layer *32nd ASME Wind Energy Symposium* (National Harbor, MD)
[23] Sørensen J N and Shen W Z 2002 *Journal of Fluids Engineering* **124** 393–399 ISSN 0098-2202
[24] Mikkelsen R 2003 *Actuator Disk Models Applied to Wind Turbines* Ph.D. thesis Technical University of Denmark
[25] Porté-Agel F, Wu Y, Lu H and Conzemius R J 2011 *Journal of Wind Engineering and Industrial Aerodynamics* **99** 154–168
[26] Wu Y and Porté-Agel F 2011 *Boundary-Layer Meteorology* **138**
[27] Jimenez A, Crespo A, Migoya E and Garcia J 2007 *Journal of Physics: Conference Series* **75**
[28] Jimenez A, Crespo A, Migoya E and J Garica, J 2008 *Environmental Research Letters* **3**
[29] Troldborg N, Larsen G C, Madsen H A, Hansen K S, Sørensen J N and Mikkelsen R 2011 *Wind Energy* **14** 859–876 ISSN 1099-1824
[30] Churchfield M, Lee S, Michalakes J and Moriarty P 2012 *Journal of Turbulence* **13**
[31] Churchfield M, Lee S and Moriarty P 2012 A large-eddy simulation of wind-plant aerodynamics *50th AIAA Aerospace Sciences Meeting* (Nashville, Tennessee)
[32] Smagorinsky J 1963 *Monthly Weather Review* **91**
[33] Selig M 2012 Propid user manual URL `http://aerospace.illinois.edu/m-selig/propid%5Cdocumentation%5CUserManual-5`
[34] Selig M and Tangler J L 1995 *Wind Engineering* **19**
[35] Jonkman J, Butterfield S, Musial W and Scott G 2009 Definition of a 5-mw reference wind turbine for offshore system development *NREL/TP-500-38060* (Colorado: National Renewable Energy Laboratory)